IRAQI BULLETIN OF GEOLOGY AND MINING
Evaluatins Impact Factor IBGM 2017 – 2018
Arcif: 0.0755
GIF: 0.936

Iraqi Bulletin of Geology and Mining *Vol.16, No.1, 2020* *p 79 – 103*

REDOX INDICATORS IN OCEANIC SEDIMENTS: A CASE STUDY OF THE ANOXIC EVENT 2 IN THE BOHEMIAN CRETACEOUS BASIN, CZECH REPUBLIC

Khaldoun S. Al-Bassam

Received: 06/ 06/ 2019, Accepted: 05/ 08/ 2019
Keywords: Anoxia; Redox-sensitive elements; Stable isotopes; Fossil bacteria; Oceanic Anoxic Event 2

ABSTRACT

One of the most expressive and well documented oceanic anoxic events; the OAE 2, is preserved at the Cenomanian/ Turonian boundary in the Pecínov section of the Bohemian Cretaceous Basin in the Czech Republic. This study aims at recording and discussing the impact of this oceanic anoxia on some potential redox parameters in the sediments of this event. It is focused on the behavior of redox-sensitive chemical elements, stable carbon and sulfur isotopes and type of fossil bacteria in the black marine mudstones and phosphate nodules deposited during the OAE 2. The results show variable concentrations of redox-sensitive elements relative to average shale, negative values of $\delta^{13}C$ in CO_3-apatite and $\delta^{34}S$ in pyrite in addition to dominant sulfur-reducing fossil bacteria. The mudstones are depleted in organic carbon and hence some trace elements (e.g., Cd, Zn, Cu and Co), usually associated with organic matter, are not significant as redox indicators in the case studied. The most prominent geochemical indicators of anoxia are expressed in the elevated Ce-anomaly and Ce/La ratio, and depleted Mn concentrations found in all samples, with the phosphate nodules holding the highest anoxic indicators. The stratigraphic correlation of geochemical redox parameters with the $\delta^{13}C_{org}$ curve at the Pecínov section shows general compatibility with some exceptions; two $\delta^{13}C_{org}$ excursions have their signature in some geochemical redox indicators. The OAE 2 section at the Pecínov quarry represents an extreme case of reduced concentrations of organic carbon and most redox-sensitive elements relative to other OAE 2 sequences in Europe and the Atlantic Ocean, which can indicate frequent oxygenation events caused by sea-level fluctuation during deposition, marked by bioturbated surfaces.

دلائل الاكسده والاختزال في الرواسب البحرية: دراسة حالة الحدث البحري الاختزالي-2 في الحوض البوهيمي الطباشيري، جمهورية الجيك

خلدون صبحي البصام

المستخلص

يعتبر الحدث البحري الاختزالي 2 من أكثر الأحداث الاختزالية البحرية دراسة وتوثيقا وآثاره محفوظة في الحدود بين عصري السينوماني والتوروني في مقطع بيشينوف ضمن الحوض البوهيمي الطباشيري في جمهورية الجيك. تهدف هذه الدراسة الى تسجيل ومناقشة عدد من المؤشرات ذات الدلالة في الرواسب التي شهدت هذا الحدث وتركز على تصرف بعض العناصر الكيميائية الدالة على ظروف الأكسدة والاختزال والنظائر المستقرة للكاربون ($\delta^{13}C$) والكبريت ($\delta^{34}S$) ونوع مستحاثات البكتريا السائدة في عينات من صخور الطين السوداء وعقد الفوسفات المترسبة ضمن تلك الفترة. تشير النتائج الى تراكيز متغيرة من العناصر الدالة قياسا على تراكيزها في صخور السجيل في العالم وأقل من تراكيزها في السجيل الأسود المرتبط بهذا الحدث الاختزالي فضلا عن قيم سالبة لنظائر الكاربون في معدن الأباتايت ونظائر الكبريت في

Czech Geological Survey, Prague, Czech Republic, e-mail: albassam703@gmail.com

معدن البايرايت مع هيمنة البكتريا المختزلة للكبريت على بقية المستحاثات المايكروبية. تحتوي هذه الصخور الطينية السوداء على تراكيز قليلة من الكاربون العضوي مما قلل من دلالة بعض العناصر المتأثرة بظروف الأكسدة والاختزال مثل الكادميوم والزنك والنحاس والكوبلت التي تتركز عادة في المواد العضوية في مثل هذه الصخور. تمثل شاذة السيريوم (Ce-anomaly) ونسبة السيريوم الى اللانثانم (Ce/La ratio) وشحة تركيز المنغنيز أهم الدلائل الجيوكيميائية على الظروف الاختزالية في كافة العينات مع تميز واضح للعقد الفوسفاتية لاحتوائها على أعلى المؤشرات في هذا المجال. بينت مضاهاة المعطيات الجيوكيميائية الدالة على الأكسدة والاختزال مع منحني نظائر الكاربون في المواد العضوية تناسقا عاما مع بعض الاستثناءات حيث ان اثنتين من شواذ نظائر الكاربون الموجبة تتفق مع دلائل جيوكيميائية دالة على الاختزال. يمثل المقطع في مقلع بيشينوف حالة متطرفة في شحة العناصر الكيميائية التي تتركز عادة في الظروف الاختزالية قياسا على مقاطع مماثلة في أوربا والمحيط الأطلسي مما يشير الى فترات متكررة من الأكسدة تعرض لها العمود الترسيبي بسبب تذبذب مستوى سطح البحر خلال تلك الفترة والتي تركت اثارها في عدة سطوح متعكرة أحيائياً.

INTRODUCTION

The Oceanic Anoxic Event 2 (OAE 2), dated at ~94 – 93 Ma (Mitchell *et al*., 2008), is considered one of the most expressive global oceanic anoxic events of the Cretaceous (Kerr, 1998; Jarvis *et al*., 2011; Gangl *et al*., 2019). It has been recognized in Asia, Africa, Europe, North America, New Zealand and the deep drilling legs at the Atlantic and Indian oceans (Schlanger and Jenkyns, 1976 and references therein). It was identified in Iraq as the black and organic carbon-rich shale of the Gulneri Formation (Cenomanian – Turonian) (Al-Dulaimy and Awadh, 2007; Al-Sheikhly *et al*., 2015) and in the Czech Republic within the Peruc-Korycany Formation (Cenomanian) and the Bílá Hora Formation (Lower Turonian) (Uličný, *et al.* 1997). This globally-recognized event lasted ~440 kyr (Vogt *et al*., 2008) and coincided with green house climate, high sea-level (Uličný *et al*., 1997), mass extinction of fauna (Kauffman, 1984; Elder, 1989) and burial of vast amounts of marine organic matter in all ocean basins, often preserved as 'black shales' (Schlanger and Jenkyns, 1976; Kuroda *et al*., 2007; Adams *et al*., 2010). This anoxic event was accompanied by high weathering rates, increased temperatures and removal of atmospheric CO_2 (e.g., Pogge von Strandmann *et al*., 2013; Du Vivier *et al*., 2014).

The OAE 2 usually shows its signature as a highly condensed section of organic-rich sediments and a globally recognized stable carbon isotopic excursion(s), which is believed to represent one of the most extreme carbon cycle perturbations of the last 100 Myr (Erbacher *et al*., 1996; Jarvis *et al*., 2006; Forster *et al*., 2007). The positive carbon isotope excursion most likely reflects increased carbon burial due to enhanced biological production (Jarvis *et al*., 2011) and has been identified (as $\delta^{13}C$) in both carbonates (2.5 to 3.0 ‰) and organic matter (2.6 to 6.0 ‰) (e.g. Turgeon and Brumsack, 2006; Jarvis *et al*., 2006; El-Shazly *et al*., 2011). The positive shifts in the $\delta^{13}C$ indicate burial of large amounts of ^{12}C-enriched organic carbon, leaving an isotopically heavier carbon source (Arthur *et al*., 1985, 1988). Consequently, the widespread removal of isotopically light organic carbon into black shales during the Cenomanian/ Turonian (C/T) event, led to ^{13}C enrichments of the oceanic and atmospheric CO_2 reservoirs (Scholle and Arthur, 1980; Arthur *et al*., 1987).

Attempts have been made to study trace elements behavior at the C/T boundary. Orth *et al*. (1988, 1993) reported iridium (Ir) peaks associated with elevated concentrations of Cr, Sc, Mn and other elements in the Upper Cenomanian and attributed this enrichment to extensive submarine volcanism. Pratt *et al.* (1991) focused on the behavior of Mn in the late Cenomanian as a redox indicator. Curiale (1993) found conspicuous U and Th spikes in a thin horizon at the C/T boundary in New Mexico and attributed them to secondary enrichment resulting from adsorption onto clay minerals. Turgeon and Brumsack (2006) studied the C/T boundary in the Umbria-Marche Basin of Italy by the analysis of redox-sensitive and/ or

sulfide-residing minor elements and found many of them to be strongly enriched in the C_{org}-rich sediments. High Zn concentrations were suggested by Turgeon and Brumsack (2006) to be due to elevated submarine hydrothermal activity during that time interval while high Ba and P concentrations have been considered to indicate high biologic productivity and nutrient availability. Al-Dulaimy and Awadh (2007) analysed Mn, Ni, Cr, Sr and Rb in the OAE 2 glauconitic black shale sequence of the Gulneri Formation in NE Iraq and found indications of euxinic environment, based on depleted Mn concentrations and Ni/Cr ratio.

Hetzel *et al.* (2006 and 2009) studied the geochemistry of black sediments of the OAE 2 in the samples recovered from the Ocean Drilling Program (ODP Leg 207) at the Demerara Rise in the tropical Atlantic and reported relative enrichment of redox-sensitive and stable sulfide forming trace elements, but depletion in Mn concentration. Furthermore, Hetzel *et al.* (2011) studied the trace elements geochemistry in the black shales at the Cenomanian – Turonian boundary in Wunstorf (northern Germany) and suggested suboxic rather than euxinic conditions at the sediment-water interface, allowing deposition of Mn or Fe oxyhydroxides. They proposed that increased productivity and oxygen deficiency resulted in the burial of organic matter and intensified reducing conditions just below the sediment-water interface, leading to formation of Fe sulphides.

In the Bohemian Cretaceous Basin (BCB), studies dealing with trace elements geochemistry along the C/T boundary are rather scarce. Dobeš *et al.* (1987) reported on the enrichment of REE in phosphate-bearing strata of Turonian age. Uličný *et al*. (1997) studied the abundance of Ir, Sc, Cr, V and other metals, reported in earlier works as forming anomalous concentrations in the C/T boundary interval, and showed no enrichment in the Bohemian section. Anomalous concentrations of Mn at the base of the Turonian deposits were explained by Uličný *et al.* (1997) to be due to diagenetic incorporation of Mn into siderite. In a recent study, Al-Bassam and Magna (2018) and Al-Bassam *et al.* (2019) made detailed analyses of REE and other trace elements in various phosphate components and glauconitic siliciclasts across the C/T boundary.

The present contribution is based upon samples and analytical results of black mudstones and phosphate nodules collected from the Upper Cenomanian – Lower Turonian sequence at the Pecínov section. The same samples have been previously analysed for trace and rare earth elements (Al-Bassam and Magna, 2018 and Al-Bassam *et al.*, 2019), stable carbon isotopes of CO_3 structurally bound to carbonate-fluorapatite (CFA) in the phosphate nodules (Al-Bassam, 2018) and characterization of fossil bacteria in these nodules (Al-Bassam and Halodová, 2018). The aim of this study is to detect and characterize the impact of the OAE 2 in the Pecínov section on the behavior of redox-sensitive elements and some geochemical indices in addition to other criteria of anoxia and to compare the results with some other OAE 2 sections of the world.

GEOLOGICAL SETTING

The BCB was developed in the mid-Cretaceous by the reactivation of a fault system in the Variscan basement of the Bohemian Massif. It formed an intracontinental basin and a seaway connecting the North Sea with the Tethys Ocean (Uličný, 1997; 2001; Uličný *et al*., 2009). It extends in the Czech Republic from Brno in E Moravia across Bohemia to the N and W of Prague (Fig.1). Sedimentation within the BCB began during Late Albian or earliest Cenomanian (Valečka and Skoček, 1991), with displaced fault zones creating topographical lows adjacent to erosional source areas (Kear *et al*., 2013).

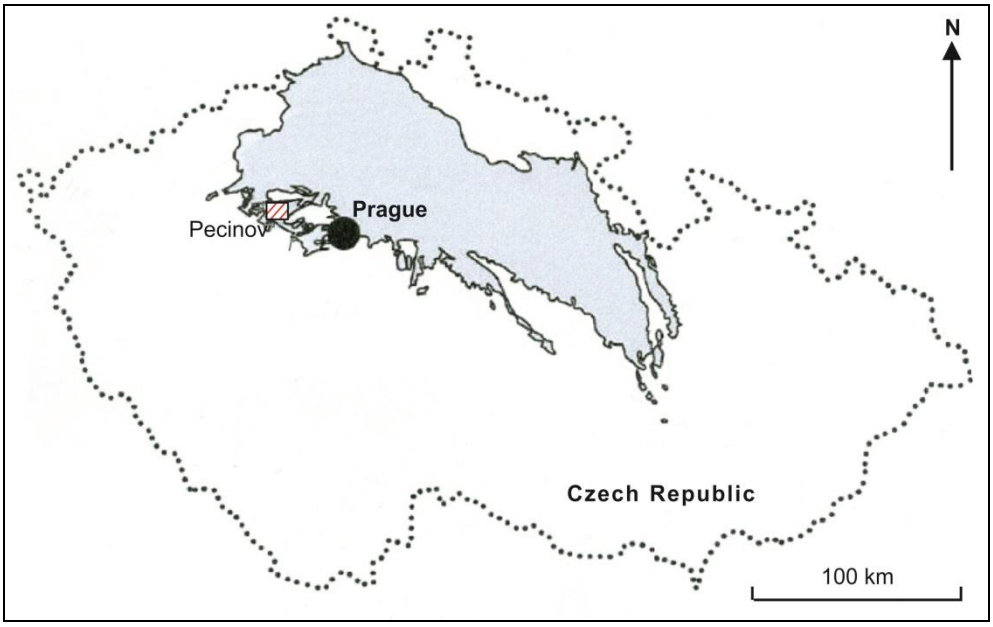

Fig.1: Extension of the Bohemian Cretaceous Basin (BCB) in the Czech Republic (light blue color) and location of the Pecínov quarry (modified after Košťák *et al*., 2018)

The Cenomanian – Lower Turonian sequence in the BCB is represented by the Peruc-Korycany Formation (Cenomanian) and the Bílá Hora Formation (Lower Turonian) (Čech *et al*., 2005; Košťák *et al*., 2018). The Peruc-Korycany Formation consists of three members: Peruc and Korycany members (Čech *et al*., 1980) and Pecínov Member (Uličný, 1997). The C/T boundary in the BCB, as documented in the Pecínov quarry section, is marked by stratigraphic condensation and erosional unconformity (Uličný *et al*., 1997). The Pecínov Member (Upper Cenomanian) was reported by Uličný (1997) to consist of four units (P1 – P4), comprised of glauconitic dark gray siltstone and mudstone and includes several omission surfaces marked by bioturbation structures and borings (Fig.2). The overlying Bílá Hora Formation (Lower Turonian) was divided by Čech *et al.* (1980) into four units (BH1 – BH4). The lower unit (BH1) is comprised of dark gray or black highly glauconitic mudstone with abundant brown phosphate nodules (Fig.2). The contact between unit P4 and unit BH1 is erosional and considered to represent the C/T boundary in this section, but with the uppermost part of Unit P4 missing due to erosion (Košťák *et al*., 2018).

The OAE 2 manifestation in the Pecínov section is marked by dark gray 6 – 7 m thick mudstone alternations (Fig.3) separated by several bioturbated omission surfaces The OAE 2 zone of influence includes units P1–P4 of the Pecínov Member and Unit BH1 of the Bílá Hora Formation (Košťák *et al*., 2018). The phosphate nodules in unit BH1 (Fig.4) are believed to have been reworked from the underlying units and mechanically emplaced at the base of the Turonian sequence (Laurin, 1996; Uličný *et al*., 1997; Al-Bassam and Magna, 2018).

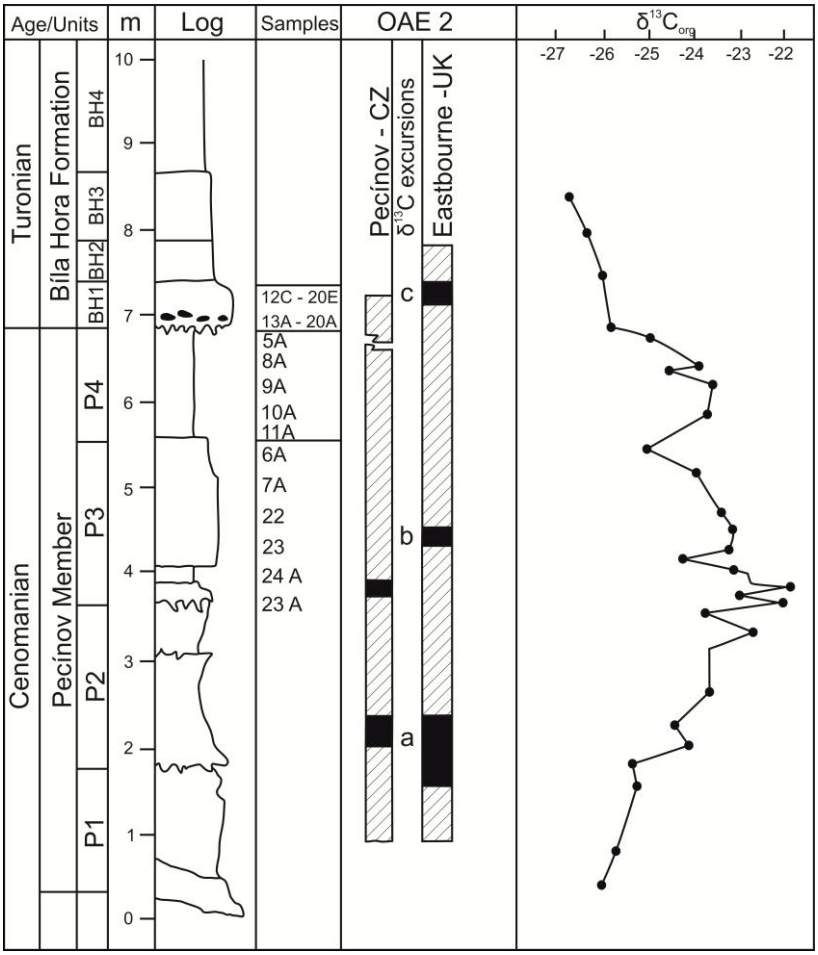

Fig.2: Stratigraphic columnar section at the Pecínov quarry (Uličný *et al*., 1997), δ $^{13}C_{org}$ curve (modified after Košťák *et al*., 2018) and samples location of the present study. (Samples 12C – 20E are 8 mudstone samples of Unit BH1 and samples 13A – 20A are 9 phosphate nodules samples in the same unit (see Tables 1, 2 and 3 for details)

Fig.3: Working face at the Pecínov quarry showing the black sequence of the OAE 2

Fig.4: Brown phosphate nodule in the mudstones of Unit BH1 showing bleached periphery

MATERIALS AND METHODS

The samples used in the present study cover the upper 4 m of the OAE 2 section in the Pecínov quarry. They include 19 mudstones and 9 phosphate nodules. The samples were collected from the upper part of the Pecínov Member (Units P3 and P4; 11 samples) and the lowermost part of the Bílá Hora Formation (Unit BH1; 8 mudstone samples and 9 phosphate nodules samples) (Fig.2). The raw chemical analysis of some major, trace and rare earth elements adapted for this study (Tables 1 – 4) are extracted from Al-Bassam and Magna (2018) and Al-Bassam *et al*., 2019), and the isotopes results are reported in Al-Bassam (2018).

All analytical procedures and instrumental analyses were performed at the Czech Geological Survey (CGS). The mineralogy was determined on the basis of combined bulk-rock chemical analysis, individual mineral phase analysis by energy dispersive microanalysis (EDX) system, X-ray diffraction (XRD) results and optical microscopy observations. The clay minerals were identified by XRD analysis of the clay fraction (-2µm). Chemical analysis of major oxides was carried out following conventional wet chemistry procedures of CGS (Dempírová *et al*., 2010). Trace element concentrations were measured using an Agilent 7900x ICPMS, housed at CGS, using Basalt BHVO-2 (USGS) and phosphate-rich sample IC10D (Ackerman *et al.,* 2017) for quality control. Detailed examination and microanalysis of the samples was carried out on carbon-coated polished sections using an FEG-SEM Tescan MIRA 3GMU scanning electron microscope (SEM) supplied with EDX system. Carbon stable isotopes in structural CO_3 of apatite were determined using standard vacuum H_3PO_4 digestion followed by measurement of evolved CO_2 by a Finnigan MAT 251 mass spectrometer using the method of McCrea (1950) and the data are reported relative to the international Vienna Pee Dee Belemnite (VPDB) standard. The reproducibility of the analysis is estimated as better than 0.05‰. The $^{34}S/^{32}S$ ratio is reported relative to Canyon Diablo Troilite (CDT). The analytical uncertainty for ^{34}S values is estimated at ± 0.2‰ (2SD). Interelement correlation coefficients were extracted using Spearman method.

Table 1: Significant elements and redox-sensitive indicators in the Upper Cenomanian mudstones in the Pecínov section*

Unit	**Pecínov Member-Unit P3**						**Pecínov Member-Unit P4**				
Sample no.	**23A**	**24A**	**23**	**22**	**7A**	**6A**	**11A**	**10A**	**9A**	**8A**	**5A**
Ti %	0.40	0.58	0.55	0.56	0.45	0.44	0.43	0.45	0.44	0.44	0.41
Al %	6.76	13.85	8.42	6.73	7.39	7.85	8.98	9.61	8.16	8.73	8.61
Fe^{3+} %	2.06	1.36	2.07	1.71	2.42	2.47	2.63	2.72	2.25	2.75	2.88
Fe^{2+} %	0.24	0.16	0.23	0.20	1.32	0.46	0.53	0.51	1.12	1.10	0.71
TOC %	0.89	0.56	0.67	0.57	0.75	0.63	0.52	0.56	0.62	0.79	0.48
S-tot. %	0.41	0.55	0.61	0.84	0.83	0.72	1.03	0.89	0.88	1.23	0.71
Mn ppm	85	54	39	31	178	85	132	139	139	185	100
Co ppm	12.5	7.2	7.0	6.8	6.5	6.2	7.3	7.1	6.2	6.0	6.9
Cu ppm	11.1	83.2	22.4	9.4	83.7	17.5	27.0	14.7	29.0	23.7	41.2
Ni ppm	61.7	21.4	20.3	19.6	22.6	19.5	21.5	21.6	20.2	19.4	20.3
Zn ppm	20.5	56.4	26.3	77.4	44.5	39.4	44.3	57.2	48.9	50.2	48.9
Cd ppm	0.13	0.17	0.19	0.16	0.17	0.16	0.18	0.18	0.17	0.15	0.16
La ppm	124	30.9	29.0	26.5	24.9	27.5	27.6	27.3	25.2	24.2	23.9
Ce ppm	873	60.5	67.6	62.5	58.7	62.8	60.6	60.8	57.8	55.1	51.4
Nd ppm	558	27.8	26.6	24.7	22.1	24.1	23.1	22.6	21.7	20.6	19.7
Fe^{2+}/Fe-tot.	0.10	0.11	0.10	0.10	0.35	0.16	0.17	0.16	0.33	0.29	0.20
Fe-tot./Al	0.34	0.11	0.27	0.28	0.51	0.37	0.35	0.34	0.41	0.44	0.42
Mn/Al	12.6	3.9	4.6	4.6	24.1	10.8	14.7	14.5	17.0	21.2	27.0
Co/Al	1.9	0.52	0.83	1.0	0.88	0.89	0.81	0.74	0.76	0.69	0.80
Cu/Al	1.6	6.0	2.7	1.4	11.3	2.2	3.0	1.5	3.6	2.7	4.8
Ni/Al	9.1	1.6	2.4	2.9	3.1	2.5	2.4	2.3	2.5	2.2	2.4
Zn/Al	3.0	4.1	3.1	11.5	6.0	5.0	4.9	6.0	6.0	5.8	5.7
Cd/Al	0.019	0.012	0.022	0.023	0.023	0.02	0.020	0.019	0.021	0.018	0.019
Mn/Ti	212	64.5	70.9	55.4	396	193	307	309	316	420	244
Co/Ti	31.3	12.4	12.7	12.1	14.4	14.1	17.0	15.8	14.1	13.6	16.8
Cu/Ti	27.8	143	40.7	16.8	186	39.8	62.8	32.7	65.9	53.9	100
Ni/Ti	154	36.9	36.9	25.0	50.2	44.3	50.0	48.0	45.9	44.1	49.5
Zn/Ti	51.3	97.2	47.8	138	98.9	89.5	103	127	111	114	119
Cd/Ti	0.33	0.29	0.35	0.29	0.38	0.36	0.42	0.40	0.39	0.34	0.39
Ce/La	7.02	1.96	2.33	2.36	2.35	2.28	2.19	2.23	2.29	2.27	2.15
Ce-anomaly**	0.18	-0.01	0.06	0.07	0.07	0.06	0.05	0.04	0.07	0.06	0.04

* Analytical data adapted from Al-Bassam and Magna, 2018 and Al-Bassam *et al*., 2019)

** Ce-anomaly calculated according to Wright *et al*. (1987) as: $\log [3 \times Ce_N / (2 \times La_N + Nd_N)]$

Table 2: Significant elements and redox-sensitive indicators in the Lower Turonian mudstones (Unit BH1) in the Pecínov section*

Sample no.	12C	13	14	16G	17F	18B	19C	20E
Ti %	0.34	0.20	0.19	0.43	0.34	0.42	0.42	0.21
Al %	7.91	4.03	4.24	8.87	7.14	9.20	8.94	4.73
Fe^{3+} %	3.82	2.93	3.26	2.48	5.59	2.14	3.13	4.66
Fe^{2+} %	1.33	2.19	3.32	0.82	0.94	2.28	0.48	1.09
TOC %	0.50	0.44	0.25	0.72	0.47	0.48	0.51	0.40
S-tot. %	0.64	0.41	0.15	0.69	3.80	0.52	1.85	0.81
Mn ppm	193	323	408	162	85	262	108	92
Co ppm	5.8	3.4	3.2	6.7	6.8	6.6	7.7	4.9
Cu ppm	20.0	6.0	12.4	15.8	13.2	81.0	12.0	6.2
Ni ppm	19.0	11.7	8.9	18.6	22.1	24.7	22.9	14.2
Zn ppm	40.2	39.6	18.2	29.4	40.7	41.9	53.4	26.3
Cd ppm	0.25	0.11	0.23	0.20	0.14	0.19	0.20	0.10
La ppm	21.9	38.7	20.2	24.7	22.5	28,8	30.2	25.7
Ce ppm	47.6	152	54.2	55.5	51.6	62.2	66.9	89.3
Nd ppm	18.4	62.7	21.5	20.8	19.8	23.8	25.4	35.9
Fe^{2+}/Fe-tot.	0.26	0.43	0.49	0.25	0.14	0.52	0.54	0.52
Fe-tot./Al	0.65	1.27	1.50	0.37	0.91	0.48	0.10	0.44
Mn/Al	24.4	80.2	96.2	18.3	11.9	28.5	12.1	19.5
Co/Al	0.74	0.85	0.74	0.76	0.95	0.72	0.86	1.03
Cu/Al	2.5	1.5	2.9	1.8	1.9	8.8	1.3	1.3
Ni/Al	2.4	2.9	2.1	2.1	3.1	2.7	2.6	3.0
Zn/Al	5.1	9.8	4.3	3.3	5.7	4.6	6.0	5.6
Cd/Al	0.032	0.027	0.054	0.023	0.020	0.021	0.022	0.021
Mn/Ti	568	1615	2147	377	250	624	257	438
Co/Ti	17.1	17.0	16.8	15.6	20.0	15.7	18.3	23.3
Cu/Ti	58.8	30.0	62.3	36.7	38.8	193	28.6	29.5
Ni/Ti	55.9	58.5	46.8	43.3	65.0	58.8	54.5	67.6
Zn/Ti	118	198	95.8	68.4	120	99.8	127	125
Cd/Ti	0.74	0.55	1.21	0.47	0.41	0.45	0.48	0.48
Ce/La	2.17	3.93	2.68	2.25	2.29	2.16	2.21	3.47
Ce-anomaly**	0.05	0.19	0.10	0.06	0.06	0.04	0.05	0.17

* Analytical data adapted from Al-Bassam and Magna, 2018 and Al-Bassam *et al*., 2019)

** Ce-anomaly calculated according to Wright *et al*. (1987) as: $\log [3 \times Ce_N / (2 \times La_N + Nd_N)]$

Table 3: Significant elements and redox-sensitive indicators in the phosphate nodules of Unit BH1*

Sample no.	13A	14A	15A	16A	17A	17E	18A	19A	20A
Ti %	0.07	0.08	0.05	0.08	0.11	0.07	0.07	0.05	0.07
Al %	1.63	1.52	1.00	0.77	1.82	1.63	1.59	1.75	1.58
Fe^{3+} %	1.39	1.98	1.51	0.91	0.60	1.27	1.34	1.48	2.93
Fe^{2+} %	0.41	0.39	0.34	0.20	0.20	0.42	0.45	0.30	0.23
TOC %	0.74	0.82	1.06	0.99	0.91	0.71	0.95	0.92	0.80
S-tot. %	0.64	1.45	1.52	0.93	0.63	0.31	1.22	1.57	3.33
Mn ppm	131	139	154	139	185	123	116	185	123
Co ppm	2.32	3.82	5.52	3.53	5.10	2.47	3.20	3.10	5.22
Cu ppm	8.52	12.91	14.19	6.83	7.16	12.95	9.42	68.7	8.48
Ni ppm	10.5	14.6	13.2	17.6	39.6	14.5	11.8	14.2	27.9
Zn ppm	35.5	125	103	24.2	60	4.00	93.1	81.0	19.9
Cd ppm	0.06	0.11	0.10	0.04	0.07	0.06	0.06	0.06	0.08
La ppm	93.6	87.3	79.7	87.3	93.5	74.0	87.8	102	66.1
Ce ppm	413	392	309	485	540	377	409	499	322
Nd ppm	165	147	107	191	216	150	154	199	128
Fe^{2+}/Fe-tot.	0.23	0.16	0.18	0.18	0.25	0.25	0.25	0.17	0.07
Fe-tot./Al	1.10	1.56	1.85	1.44	0.44	1.04	1.13	1.02	2.00
Mn/Al	80.4	91.5	154	181	102	95.5	73.0	106	77.9
Co/Al	1.4	2.5	5.5	4.7	2.8	1.5	2.0	1.8	3.3
Cu/Al	5.2	8.5	14.2	8.9	3.9	7.9	5.9	39.3	5.37
Ni/Al	6.4	10.1	13.2	22.9	21.7	8.9	7.4	8.1	17.7
Zn/Al	21.8	82.2	104	31.4	33.0	2.5	58.5	56.3	12.6
Cd/Al	0.037	0.072	0.100	0.052	0.038	0.037	0.038	0.034	0.051
Mn/Ti	1871	1738	3080	1738	1682	1757	1657	3700	1757
Co/Ti	33.1	47.8	11.0	44.1	46.4	35.3	45.7	62.0	74.6
Cu/Ti	122	161	284	85.4	65.1	185	135	1374	121
Ni/Ti	150	183	264	221	360	210	168	283	398
Zn/Ti	464	1562	2065	302	545	57.1	1329	1620	285
Cd/Ti	0.86	1.38	2.00	0.50	0.64	0.86	0.86	1.20	1.14
Ce/La	4.41	4.49	3.88	5.56	5.78	5.09	4.66	4.88	4.87
Ce-anomaly**	0.23	0.24	0.22	0.28	0.28	0.26	0.25	0.25	0.25

*Analytical data adapted from Al-Bassam and Magna, 2018 and Al-Bassam *et al*., 2019)

** Ce-anomaly calculated according to Wright *et al*. (1987) as: $\log [3 \times Ce_N / (2 \times La_N + Nd_N)]$

Table 4: Mean and range values of significant elements and redox-sensitive indicators in the Upper Cenomanian – Lower Turonian mudstones and phosphates in the Pecínov section

Unit	P3 (6 samples)	P4 (5 samples)	BH1 (8 samples)	Average Shale*	BH1 (9 samples)
Lithology	**Mudstone**	**Mudstone**	**Mudstone**		**Phosphate**
Ti %	0.50 (0.40 – 0.58)	0.43 (0.41 – 0.45)	0.32 (0.19 – 0.44)	0.46	0.07 (0.05 – 0.11)
Al %	8.50 (6.73 – 13.85)	8.82 (8.16 – 9.61)	6.88 (4.03 – 9.20)	8.0	1.48 (0.77 – 1.82)
Fe-tot.	2.46 (1.52 – 3.74)	3.44 (3.16 – 3.85)	5.06 (3.30 – 6.58)	4.7	1.82 (0.80 – 3.16)
Fe^{3+} %	2.02 (1.36 – 2.47)	2.65 (2.25 – 2.88)	3.50 (2.14 – 5.59)		1.49 (0.60 – 2.93)
Fe^{2+} %	0.44 (0.16 – 1.32)	0.79 (0.51 – 1.12)	1.56 (0.48 – 3.32)		0.33 (0.20 – 0.45)
TOC %	0.68 (0.56 – 0.89)	0.59 0.48 – 0.79)	0.47 (0.25 – 0.72)		0.88 (0.74 – 1.06)
S-tot. %	0.66 (0.41 – 0.84)	0.95 (0.71 – 1.23)	1.11 (0.15 – 3.80)		1.29 (0.31 – 3.33)
Mn ppm	78.7 (31 – 178)	139 (100 – 185)	205 (85 – 408)	850	144 (116 – 185)
Co ppm	7.7 (6.2 – 12.5)	6.7 (6.0 – 7.3)	5.6 (3.2 – 7.7)	19	3.8 (2.3 – 5.5)
Cu ppm	37.9 (9.4 – 83.7)	27.1 (14.7 – 41.2)	20.8 (6.0 – 81.0)	45	16.6 (6.8 – 68.7)
Ni ppm	27.5 (19.5 – 61.7)	20.6 (19.4 – 21.6)	17.8 (8.9 – 24.7)	68	18.2 (10.5 – 39.6)
Zn ppm	44.1 (20.5 – 77.4)	49.9 (44.3 – 57.2)	36.2 (26.3 – 53.4)	95	60.3 (4.0 – 125)
Cd ppm	0.16 (0.13 – 0.19)	0.17 (0.15 – 0.18)	0.18 (0.10 – 0.25)	0.3	0.07 (0.04 – 0.11)
La ppm	43.9 (24.9 – 124)	25.6 (23.9 – 27.6)	26.6 (20.2 – 38.7)	41	85.7 (66.1 – 102)
Ce ppm	197.5 (60.5 – 873)	57.1 (51.4 – 60.8)	72.4 (47.6 – 152)	83	416 (309 – 540)
Nd ppm	113.7 (22.1 – 557)	21.5 (19.7 – 23.1)	45.2 (18.4 – 89.3)	38	162 (107 – 216)
Fe^{2+}/Fe-tot.	0.15 (0.1 – 0.35)	0.23 (0.16 – 0.33)	0.30 (0.13 – 0.52)		0.19 (0.07 – 0.25)
Fe-tot./Al	0.31 (0.11 – 0.51)	0.39 (0.34 – 0.44)	0.72 (0.37 – 1.5)	0.59	1.29 (0.44 – 2.0)
Mn/Al	10.1 (3.9 – 24.1)	18.9 (14.5 – 27.0)	36.6 (11.9 – 96.7)	106	107 (73 – 181)
Co/Al	1.0 (0.5 – 1.9)	0.76 (0.69 – 0.81)	0.83 (0.74 – 1.03)	2.4	2.84 (1.4 – 5.5)
Cu/Al	4.2 (1.4 – 11.3)	3.1 (1.5 – 4.8)	2.8 (1.3 – 8.8)	5.6	11.1 (3.9 – 39.3)
Ni/Al	2.6 (1.6 – 9.1)	2.3 (2.2 – 2.5)	2.6 (2.1 – 3.0)	8.5	12.9 (6.4 – 22.9)
Zn/Al	5.5 (3.0 – 11.5)	5.7 (4.9 – 6.0)	5.5 (3.3- – 9.8)	11.9	44.4 (2.5 – 103)
Cd/Al	0.020 (0.012 – 0.023)	0.019 (0.018 – 0.021)	0.028 (0.020 – 0.054)	0.038	0.051 (0.034 – 0.100)
Mn/Ti	165 (55.4 – 396)	317 (244 – 420)	784 (250 – 2147)	1848	2108 (1657 – 3700)
Co/Ti	16.2 (12.1 – 31.3)	15.5 (13.6 – 17.0)	18.0 (15.6 – 23.3)	41.3	44.4 (11.0 – 75)
Cu/Ti	75.7 (16.8 – 143)	63.1 (32.7 – 100)	59.7 (28.6 – 193)	97.8	281 (65.1 – 1374)
Ni/Ti	57.9 (25.0 – 154)	47.5 (44.1 – 50.0)	56.3 (43.3 – 67.6)	147.8	248 (149.9 – 398)
Zn/Ti	87.1 (47.8 – 138)	115 (103 – 127)	119 (68.4 – 198)	207	915 (57.1 – 2065)
Cd/Ti	0.33 (0.29 – 0.38)	0.39 (0.34 – 0.42)	0.60 (0.41 – 1.2)	0.65	1.05 (0.50 – 2.0)
Ce/La	3.1 (2.0 – 7.0)	2.2 (2.2 – 2.3)	2.7 (2.2 – 2.9)	~ 2	4.9 (3.9 – 5.8)
Ce-anomaly**	0.07 (-0.01 – 0.18)	0.05 (0.04 – 0.07)	0.09 (0.04 – 0.19)	-0.12	0.25 (0.22 – 0.28)

* Average Shale after Turekian and Wedepohl (1961); REE after Haskin and Haskin, (1966)

** Ce-anomaly calculated according to Wright *et al*. (1987) as: $\log [3 \times Ce_N / (2 \times La_N + Nd_N)]$

RESULTS AND DISCUSSION

- **Total Organic Carbon (TOC)**

Organic-rich sediments typically contain > 1 wt.% organic carbon (Tourtelot, 1979) and up to 30 – 50 wt % TOC have been observed in the OAE 2 black shales of the northern hemisphere that are indicative of locally persistent anoxic or euxinic conditions (Kuhnt *et al*., 2005; Kuypers *et al*., 2002 and Monteiro *et al*., 2012). The TOC content in the mudstone samples of this study is lower than 1 wt.%, ranging (0.48 – 0.89 wt.%) and it is decreasing upward in mean values from 0.68 wt.% in Unit P3; 0.59 wt.% in Unit P4 and to 0.47 wt.% in Unit BH1 (Tables 1 – 4). The TOC content in the mudstones of the Pecínov section is lower than other OAE 2 black shales of Germany, Italy and the Atlantic Ocean (Table 5). The highest TOC contents are found in the mudstone sample 23A (0.89 wt.%) and in the phosphate nodules (mean = 0.88 wt.%).

The low TOC concentrations in the OAE 2 sequence of the Pecínov section can be compared to similarly low TOC concentrations in the OAE 2 sections at Sawpit Gully and Mangaotane B of the continental margin of New Zealand which were considered to indicate relatively well-oxygenated depositional environments (Gangl, *et al*., 2019). Greater amount of TOC may be preserved in the sediments when there is short residence time in the oxic part of the water column and low content or complete absence of oxygen in the lower part, near sediment-water interface (Brumsack, 1989). The relatively low TOC content in the studied mudstones can be attributed to the frequent shallowing events associated with omission surfaces which resulted in intermittent oxygenation episodes throughout the OAE 2 sequence in the Pecínov section, indicated by the common presence of burrowing structures in the whole sequence (Fig.2). Shallowing events, associated with increased oxygenation are reported in many black shale deposits, indicated by erosional surfaces, cross stratification and low-angled cross bedding (e.g., Schieber, 1994).

Table 5: Total organic carbon (TOC) and some redox-sensitive elements (normalized to Al) in black mudstones of the OAE 2 in the Pecínov section compared to other localities

Redox indicators	Wunstorf-Germany[(1)]	Umbria-Marche Italy[(2)]	ODP Leg 207 Site 1258 Atlantic[(3)]	ODP Leg 207 Site 1260 Atlantic[(3)]	Pecínov Units P3 & P4 Cenomanian[(4)]	Pecínov Unit BH1 Turonian[(4)]
TOC %	1.16	2.60	17.82	12.2	0.64	0.47
Fe-tot./Al	0.82	0.80	0.76	0.80	0.34	0.72
Mn/Al	952.8	15.0	18.4	5.9	14.2	36.4
Co/Al	14.7	4.7	4.5	4.4	0.80	0.83
Cu/Al	9.8	64	24	30.5	3.9	2.8
Ni/ Al	17.7	26	59.5	73.0	2.4	2.6
Zn/Al	24.7	229	48.1	154.0	5.8	5.5

[(1)] Hetzel *et al.* (2011); [(2)] Turgeon and Brumsack (2006); [(3)] Hetzel *et al*. (2006); [(4)] Present work

- **Iron**

Iron content increases upward in the Pecínov mudstone sequence from 2.46 wt.% in Unit P3 to 3.44 wt.% in Unit P4 and 5.06 wt.% in Unit BH1 compared to 4.7 wt.% in average shale. Total Fe normalized to Al (Fe_{tot}/Al ratio) has been used as redox indicator in the sedimentary environment (Turgeon and Brumsack, 2006; Hetzel *et al*., 2009; 2011). Elevated

Fe_{tot}/Al values relative to average shale document euxinic conditions allowing reductive Fe mobilization in oxygen-depleted sediments (Hetzel, 2009). The Fe_{tot}/Al ratio in the mudstones ranges from 0.11 to 1.50, increasing in mean values from 0.31 to 0.39 and to 0.72 in units P3, P4 and BH1 respectively, compared to Fe_{tot}/Al ratio of 0.59 in average shale. Higher values are found in the phosphate nodules (mean Fe_{tot}/Al ratio = 1.29). The Fe_{tot}/Al ratios in the Pecínov mudstones are close to those found in black shales of other OAE 2 sequences in Europe and the Atlantic Ocean (Table 5).

The increase in ferrous Fe (Fe^{2+}) relative to total Fe (Fe_{tot}) content corresponds to increased oxygen deficiency in the depositional environment, where significant part of Fe^{3+} is reduced to Fe^{2+}. The Fe^{2+}/Fe_{tot} ranges from 0.1 to 0.52 in the mudstones, increasing upward in mean values from 0.15; 0.23 and 0.30 in units P3, P4 and BH1 respectively following the same trend as Fe_{tot}/Al (Table 4). Unit BH1 exhibits the widest range of Fe^{2+}/Fe_{tot} ratio; whereas the phosphate nodules and sample 23A show generally lower Fe^{2+}/Fe_{tot} ratios than the mudstone samples (Tables 1 – 4). The increase in the Fe_{tot}/Al ratio in the mudstones is attributed to the increase of Fe^{2+} content, which indicates higher oxygen deficiency upward. Ferrous Fe is mainly incorporated in glauconite and pyrite in the studied samples, whose contents increase upward in the sequence (Table 6). Glauconite indicates stagnation and reduced sedimentation rate (e.g., Ugata, 2007) and pyrite indicates increased deficiency of oxygen and increased H_2S activity, produced by the microbial reduction of marine sulfate (e.g., Arning *et al*., 2009, Hiatt *et al*., 2015). Both criteria suggest oxygen-depleted conditions increasing upward from units P3 to P4 and to BH1. The lower values of Fe^{2+}/Fe_{tot} found at the base of Unit P3 (sample 23A) and in the phosphate nodules do not necessarily indicate increased oxygenation and may be attributed to mineral constrains induced by the lower contents of glauconite and to some extent pyrite in these samples (Table 6).

Table 6: Mineralogy of the studied samples (adapted from Al-Bassam *et al*., 2019)

Minerals (modal %)	Unit P3 Sample 23A	Unit P3 Mudstones	Unit P4 Mudstones	Unit BH1 Mudstones	Unit BH1 Phosphates
Glauconite	14.8	10.7 – 31.2	27.1 – 31.0	26.2 – 37.6	4.3 – 11.8
Kaolinite + Smectite	27.9	29.2 – 63.9	33.0 – 40.3	10.7 – 37.2	1.8 – 6.0
Quartz	27.5	15.8 – 50.1	25.6 – 32.2	25.1 – 38.6	1.9 – 11.8
Pyrite	0.6	0.5 – 1.6	1.0 – 2.3	0.3 – 6.8	0.5 – 2.2
Organic-C (TOC)	0.9	0.6 – 0.7	0.5 – 0.8	0.2 – 0.7	0.7 – 1.1
Apatite	22.5	Trace	Trace	Trace	63.1 – 85.4

- **Rare Earth Elements (REE)**

The Ce-anomaly, calculated as log $[3 \times Ce_N/ (2 \times La_N + Nd_N)]$, has been widely used as redox indicator and to define the source of REE in marine sedimentary environments (e.g., Wright *et al*., 1987; Shields and Stille, 1998; German *et al*., 1991; Piper and Bau, 2013). Negative Ce-anomaly values indicate oxidizing conditions, which result from depletion of Ce or fractionation by precipitation with metallic oxides, and positive values indicate suboxic to anoxic conditions in seawater (Wright *et al*., 1987). Almost all samples collected and analysed from the OAE 2 profile in the Pecínov section (Al-Bassam and Magna, 2018) show Ce-anomaly in the anoxic field of Wright *et al*. (1987) (Fig.5). The highest Ce-anomaly values are found in the phosphate nodules (0.22 – 0.28) and in the basal part of Unit P3 (sample 23A) with 0.18. The mudstones of units P3, P4 and BH1 show generally lower values (-0.01 – 0.19) (Tables 1 – 4).

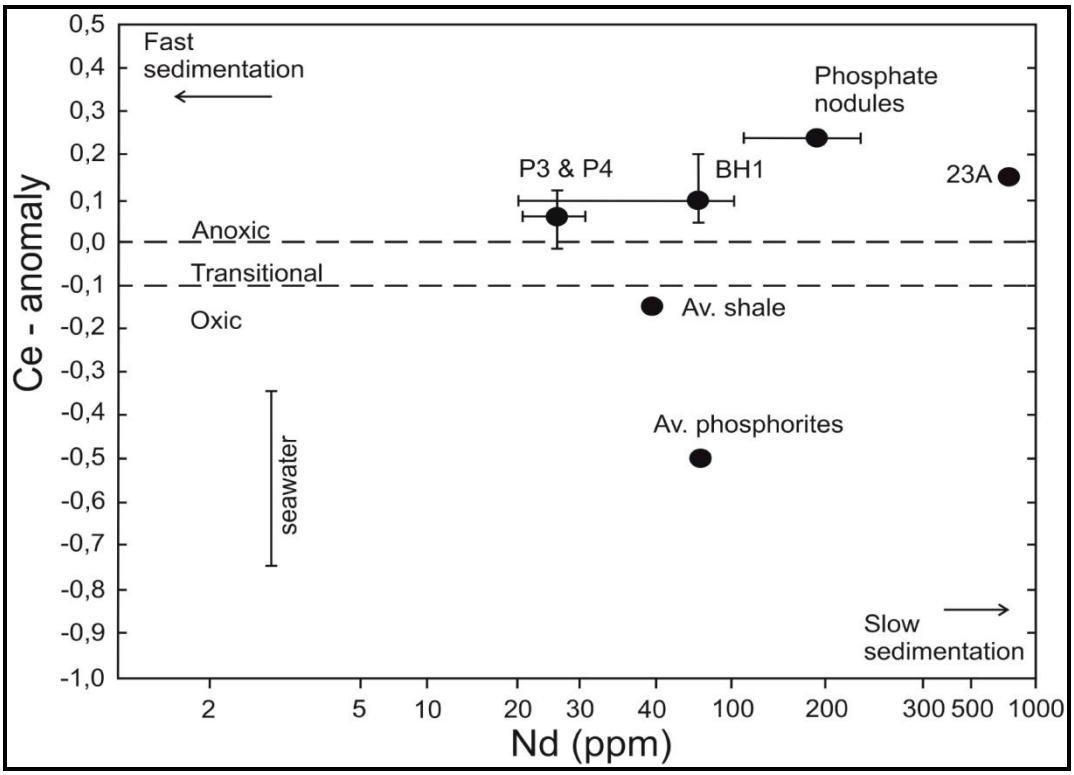

Fig.5: Ce-anomaly versus Nd concentration in the mudstones and phosphates of the present study (modified after Al-Bassam and Magna, 2018), compared to seawater (Høgdahl, *et al*., 1968), average shale (Haskin and Haskin, 1966) and average phosphorites (Altschuler, 1980), showing redox boundaries and sedimentation rates (Wright, *et al*., 1987)

The Ce/La ratio is also used as an indicator of redox conditions of the aqueous environment; the higher the Ce/La ratio the more oxygen-depleted the environment. This is well illustrated by the difference in Ce/La ~0.35 in open seawater (Høgdahl *et al*., 1968) versus Ce/La ~2 in average world shale (Haskin and Haskin, 1966). The Ce/La ratios are >2 in the entire suite and are well above values reported for average shale of (Haskin and Haskin, 1966). The mudstones of the Bílá Hora Formation (Unit BH 1) show mean Ce/La = 2.65, and the Pecínov member (units P3 and P4) shows mean Ce/La = 2.68, (Tables 4). The highest Ce/La ratio is found at the base of Unit P3 (sample 23A) of 7.02 and the phosphate nodules with a mean of 4.9 (range 3.9 – 5.8).

The Ce-anomaly values and the Ce/La ratios of the mudstones of units P3, P4 and BH1 indicate anoxic conditions throughout the Upper Cenomanian and earliest Turonian sequence in the Pecínov section (Fig.5), which is compatible with the OAE 2 zone of influence here (see Košťák *et al*., 2018). The mudstone samples from Unit BH 1 of Bílá Hora Formation show more variable values of Ce-anomaly and Ce/La ratio, which may be linked to variable, but generally suboxic, conditions of reworking during early Turonian. The phosphate nodules hosted in Unit BH1 have the largest extent of Ce-anomaly and Ce/La ratios among all samples suggesting that they were originally formed in the highest conditions of anoxia compared to the mudstones of Unit BH1, hosting them now, as well as to the mudstones of the Pecínov Member and they are comparable in this respect to sample 23A at the base of Unit P3.

- **Redox Sensitive Trace Elements**

Syn-sedimentary enrichments of redox sensitive and sulfide residing elements in various sedimentary environments have been related to oxygen-depleted bottom waters conditions (Piper, 1974; Calvert and Pedersen, 1993). They include, but not limited to, Co, Cu, Ni, Zn and Cd. On the other hand, Mn is usually depleted in black shales where Mn^{4+} is reduced to the more soluble Mn^{2+} and is consequently removed from the water column to deeper parts of the basin. The trace elements (TE's) concentrations and relevant redox indices derived from these TE's (except Mn and REE) are lower in the studied mudstones of the Pecínov section than average shale and the values of Co, Cu, Ni and Zn normalized to Al are lower than other OAE 2 black shales in Europe and the Atlantic Ocean (Table 5). However, the redox indices found in these OAE 2 black shales show highly variable values (Table 5) suggesting that there is no consistent geochemical facies characteristic of these black sediments. Nevertheless, OAE 2 section in the Pecínov section represents a remarkable case of TE's depletion coupled with depleted TOC concentrations relative to most black shales of the world. Some of the redox-sensitive TE's may have been present in the early diagenetic environment as soluble complexes with reduced sulfur species, where their mobility in anoxic sediments increases and considerable part of these elements may have subsequently diffused through the sediments (Huerta-Diaz and Morse, 1992).

The mineral constituents of the studied mudstone samples (Table 6) suggest more than one host for Mn, Co, Cu, Ni, Zn and Cd. Some of these minerals are detrital (kaolinite and smectite) and others are authigenic or early diagenetic (glauconite, apatite and pyrite). Organic material may be important as a host of some of these elements, similar to most black shales. Trace elements residing in detrital minerals may not be useful as redox indicators of the depositional environment as they only carry the geochemical signature of the source material. To overcome such problems, Al-normalized data have been often used to assess redox conditions (Turgeon and Brumsack, 2006; Hetzel, *et al*., 2006; 2009). In our case, Al is present not only in detrital clay minerals but it is a major constituent of the authigenic glauconite common in the studied mudstones. To minimize the inconsistency that might occur with Al-normalization of TE's, all redox sensitive TE's were normalized to Ti (in addition to Al), being fixed in the detrital minerals only.

Correlation between TOC and TE's is used as an indicator of paleoredox conditions by numerous authors (e.g., Cruse and Lyons, 2004; Algeo and Maynard, 2004; Algeo *et al*., 2007). The Spearman correlation coefficients in this study show variable results among the various sample groups (Tables 7a and b), but the small number of samples rendered many values below the statistical significance level. None of the redox-sensitive TE's in the Upper Cenomanian units P3 and P4 is related to TOC (Table 7a), whereas, most TE's in the Lower Turonian mudstones (Unit BH1), except Cd and Mn, show positive correlations with TOC (Table 7b). Tribovillard *et al*. (2006) pointed out that no correlation of TOC with TE's indicates that the latter were deposited with the detrital fraction under oxic-dysoxic conditions, whereas, anoxic, but not sulfidic, conditions favor strong TOC-TE's covariation. Among other possible reasons for the poor correlation between TOC and TE's in the mudstones of units P3 and P4 may be the narrow range of TOC concentration in these units and the small number of samples (Table 1), making statistical correlation insignificant.

– ***Manganese*****:** Low Mn concentrations are found in the mudstones of all units ranging 31 – 408 ppm, increasing upward in mean values from 78.7, to 139 and 205 ppm in units P3, P4 and BH1, respectively compared to 850 ppm in average shale (Tables 1 – 4). The mean value of Mn/Al and Mn/Ti ratios increase upward in units P3, P4 and BH1 but they are much

lower than those in average shale of 106 and 1848 respectively (Table 4). Unit BH1 shows wider range and higher values of Mn/Al and Mn/Ti ratios (11.9 – 96.7 and 250 – 2147 respectively) compared to the underlying units. The highest Mn/Al and Mn/Ti ratios are found in the phosphate nodules (mean = 107 and 2108, respectively (Table 4). Authigenic glauconite is the main host of Mn in the mudstones of the Upper Cenomanian part of the sequence (Al-Bassam *et al*., 2019), suggested in the present study by the significant positive correlation of Mn with Fe_2O_3, FeO and MgO (Table 7a). In the Lower Turonian part of the section this association is demonstrated in the covariation of Mn with FeO only, which may also point to pyrite and glauconite as hosts (Table 7b). Apatite may be another host of Mn in this part of the sequence, demonstrated in the positive correlation with CaO and higher values of Mn/Al and Mn/Ti ratios in the phosphate nodules (Table 4).

Table 7: Correlation coefficients of trace elements with major components (Processed from analytical data reported in Al-Bassam *et al*., 2019)

7a: Pecínov Member mudstones (r ~ 0.6)										
	TiO_2	**Al_2O_3**	**Fe_2O_3**	**FeO**	**CaO**	**MgO**	**K_2O**	**P_2O_5**	**TOC**	**Total S**
Mn			0.67	0.89	0.60	0.63	0.53			0.64
Co								0.42		
Cu				0.53		0.41	0.36			
Ni								0.54		
Zn	0.49									0.44
Cd		0.38	0.55	0.38	0.49					0.70
7b: Bílá Hora Formation mudstones (r ~ 0.7)										
	TiO_2	**Al_2O_3**	**Fe_2O_3**	**FeO**	**CaO**	**MgO**	**K_2O**	**P_2O_5**	**TOC**	**Total S**
Mn				0.75	0.70		0.32	0.41		
Co	0.72	0.70							0.79	0.69
Cu	0.64	0.69							0.67	
Ni	0.74	0.84							0.71	0.54
Zn	0.34	0.41							0.70	0.72
Cd	0.47		0.51						0.45	

The Mn/Al and Mn/Ti ratios of all mudstone units are lower than those in average shale, but the former is comparable to Mn/Al ratios found in OAE 2 black shale sequences in Italy and the Atlantic Ocean (Table 5). The depleted Mn concentrations in the studied mudstones, relative to average shale, point to strong oxygen deficiency during deposition (e.g., Turgeon and Brumsack, 2006; Marlof, 2014), and demonstrates the suboxic conditions prevailed during the OAE 2 in the Pecínov section. The deficiency of Mn suggests that it was either reduced within the water column before sedimentation or upon early diagenesis in an environment open to dissolved Mn^{2+} loss as provided by an expanded oxygen-minimum zone, like the modern upwelling zones off Peru (Böning *et al*., 2004) or in the Gulf of California (Brumsack, 1989). Similar mobilization of Mn at the OAE 2 was found in the Northwest Australian margin (Thurow *et al*., 1992) and in the Atlantic Ocean deep drilling project (Hetzel *et al*., 2009).

– ***Cobalt*:** Almost all mudstone samples within the OAE 2 profile show low Co concentrations (< 10 ppm) compared to 19 ppm in average shale. The Co concentrations vary within a relatively wide range in the mudstones (3.2 – 12.5 ppm). Lower Co concentrations and narrower range are found in the phosphate nodules (2.3 – 5.5 ppm). The Co/Al Co/Ti ratios for most mudstone samples (except 23A) are generally < 1.0 and < 25 respectively

compared to ~2.4 and ~41 in average shale (Table 4) and the Co/Al ratio is much lower than those reported in other OAE 2 sequences (Table 5). Sample 23A, at the base of Unit P3, shows the highest Co concentration and Co/Al and Co/Ti ratios among all mudstone samples (Table 1). Cobalt shows weak and insignificant correlation with the major components in the mudstones of units P3 and P4, whereas, in the mudstones of Unit BH1 it is related to TOC, Total S, TiO_2 and Al_2O_3, suggesting multiple hosts, including organic matter, pyrite and detrital clay minerals respectively. The most variable and highest Co/Al and Co/Ti ratios are found in the phosphate nodules, ranging (1.4 – 5.5) and (11.0 – 74.6), respectively (Tables 3 and 4) suggesting variable redox conditions, but generally more reducing in the phosphogenic environment than that of the mudstones.

The low Co concentrations, Co/Al and Co/Ti ratios found in the analysed mudstones suggest that most of the Co was amenable for diagenetic mobilization from the original hosts of Co-bearing Mn-Fe oxy-hydroxide phases. Hetzel (2009) suggested that under oxygen depleted conditions, cobalt, associated with Mn-and Fe-oxyhydroxides, would be mobilized and transported away. Similar cases have been noticed in upwelling sediments such as those in the Gulf of California (Brumsack, 1989) or the Peruvian margin (Böning *et al*., 2004). The higher Co/Al and Co/Ti ratios found in the phosphate nodules and in sample 23A may be related to the elevated TOC and phosphate contents of these samples and indicate relatively higher oxygen deficiency during deposition.

– ***Copper*****:** Copper concentrations in the studied mudstone samples are generally lower than average shale and vary from 9.4 to 83.7 ppm with mean values decreasing upward from 37.9 ppm in Unit P3 to 27.1 ppm in Unit P4 and to 20.8 ppm in Unit BH1 compared to 45 ppm Cu in average shale (Table 4). The same trend is demonstrated in the Cu/Al and Cu/Ti ratios; where the former decreases from 4.2 to 3.1 to 2.8, and the latter decreases from 75.7 to 63.1 and to 59.7 in units P3, P4 and BH1, respectively compared to 5.6 and 97.8 in average shale (Table 4). The Cu/Al ratios in the studied mudstones are much lower than those reported in other OAE 2 black shales (Table 5), whereas the phosphate nodules exhibit the highest values of Cu/Al and Cu/Ti ratios at 11.1 and 281, respectively.

The correlation coefficients (Table 7a) show that in the Pecínov units Cu has weak and insignificant correlation with the main components, whereas in the Bílá Hora unit it is positively correlated with Al_2O_3, TiO_2 and TOC (Table 7b), suggesting that Cu is fractionated between detrital clay minerals and organic matter. There is no specific enrichment of copper in the studied sequence that can be related to suboxic conditions, except in some mudstone samples (7A and 24A) and in most of the phosphate nodules which show elevated values of Cu/Al and Cu/Ti ratios relative to the mudstone samples, and support other parameters in suggesting higher oxygen deficiency during phosphogenesis.

– ***Nickel:*** Lower than average shale concentrations of Ni are found in the mudstone samples, ranging from 8.9 ppm to 61.7 ppm compared to 68 ppm in average shale. The highest concentration is found at the base of Unit P3 (sample 23A) and a wider range (8.9 – 24.7 ppm) and a lower mean value (17.8 ppm) is found in the mudstones of Unit BH1 (Tables 1 – 4). The Ni/Al and Ni/Ti ratios in the mudstones are generally lower (range 1.6 – 9.1 and 25.0 – 154) than those in average shale of 8.5 and 147.8, respectively. Nickel concentration, Ni/Al and Ni/Ti ratios do not show specific trends in the Pecínov mudstones with the exceptionally high values recorded at the base of Unit P3, where higher Ni/Al and Ni/Ti ratios are found in sample 23A, exceeding those in average shale (Table 1). The highest

of the Ni/Al and Ni/Ti ratios are found in the phosphate nodules reaching up to 22.9 and 398 respectively (Table 3).

In units P3 and P4, Ni is insignificantly correlated with the major components except a weak positive correlation (r = 0.54) with P_2O_5 (Table 7a), whereas in Unit BH1 it is associated with detrital clay minerals and organic matter as suggested by the significant correlation coefficients of Ni with TiO_2, Al_2O_3 and TOC (Table 7b). The high Ni concentration at the base of Unit P3 (sample 23A) relative to other mudstone samples is coupled with higher concentration of Co and both may be related to the high content of apatite at the omission surface between units P2 and P3 (Fig.2 and Table 6). The Ni/Al ratio is lower than those in comparable OAE 2 black shales (Table 5). Significant part of Ni^{2+} in the detritus brought to the depositional basin of the BCB was probably bound to Fe- oxyhydroxides, and was partly mobilized away from the system in the early stages of diagenesis. The remaining part of Ni was trapped in apatite, indicated by the much higher Ni/Al and Ni/Ti ratios in the phosphate nodules (Table 3) and suggesting reducing conditions below sediment-water interface where the phosphate precipitated.

– ***Zinc*****:** Zinc concentrations in the mudstones are ranging between 20.5 and 77.4 ppm compared to 95 ppm in average shale (Table 4). Lower mean value of 36.2 ppm is found in Unit BH1 compared to (44.1 and 49.9) ppm in units P3 and P4, respectively. Zn/Al and Zn/Ti ratios range from 3.0 to 11.5 and 47.8 to 198 in the mudstones of all units compared to 11.9 and 207 in average shale respectively. Unit BH1 exhibits the widest range of Zn concentration, Zn/Al and Zn/Ti ratios (Table 4). The lowest Zn/Al value is found sample 23A at the base of Unit P3. The phosphate nodules are relatively enriched in Zn and show much higher mean values of Zn/Al and Zn/Ti ratios (44.1 and 915, respectively) than the mudstones.

The lower Zn concentrations in the Cenomanian and Turonian mudstones relative to average shale is in harmony with the low concentrations of other redox sensitive TE's analysed in this sequence including Mn, Co, Cu, Ni and Cd. The same behavior can be noticed in the Zn/Al and Zn/Ti ratios in all mudstone samples. A distinct decrease in Zn/Al ratios during OAE 2 was also observed in the Demerara Rise sections (Hetzel *et al*., 2009) compared to other Cretaceous black shales, known to be highly enriched in Zn (Brumsack, 2006; Hetzel, *et al*., 2006). The correlation coefficient of Zn is insignificant with all major components in units P3 and P4, except weak positive (below significance level) correlation with total sulfur and TiO_2 (Table 7a) which might suggest pyrite and detrital clay minerals as hosts respectively. On the other hand, organic matter and pyrite can be suggested as the main hosts of Zn in the mudstones of Unit BH1, based on the significant positive correlation of Zn with TOC and Total S (Table 7b). The higher Zn/Al and Zn/Ti ratios found in the phosphate nodules (mean = 44.4 and 915 respectively) indicate Zn enrichment in the phosphate nodules and attests for the suboxic conditions of phosphogenesis. Zinc in these nodules is possibly replacing Ca^{2+} in the apatite structure and/or trapped in organic matter.

– ***Cadmium*****:** Cadmium concentrations, Cd/Al and Cd/Ti ratios are lower in the studied mudstones than those of average shale. Cadmium concentrations range (0.10 – 0.25 ppm) in all mudstone units compared to (0.3 ppm) in average shale. The lowest Cd concentration among the Pecínov Member samples (0.13 ppm) is found in sample 23A (Table 1). The Cd concentration, Cd/Al and Cd/Ti ratios show higher mean values and wider range in the mudstones of Unit BH1 (Table 2). The phosphate nodules contain lower Cd concentrations, but higher Cd/Al and Cd/Ti ratios than the mudstones (Table 3). Cadmium show insignificant

correlation with most major components in the studied mudstones, except with Total S in the Pecínov Member samples, pointing towards pyrite as a host (Tables 7a and b). However, several hosts of Cd in the mudstones can be suggested based on Cd geochemical affinity and mineralogy of the samples. These may include apatite, pyrite, smectite and organic matter. The possibility of multiple host minerals of Cd in these mudstones and the small number of samples may have reduced the significance of most correlation coefficients.

The depleted concentration of Cd in the mudstones of the OAE 2 section at the Pecínov quarry is compatible with the trend noticed in the other redox sensitive trace elements discussed in this study and demonstrates a remarkable case of TE's depletion among black shales deposited in suboxic conditions. The deficiency in most redox sensitive TE's can be attributed to the relatively low contents of organic matter and sulfide minerals in the depositional and early diagenetic environments, caused by frequent short oxygenation episodes during the OAE 2 in the Pecínov section. Moreover, even in anoxic environments, cadmium and other redox sensitive elements may form soluble complexes with reduced sulfur species, increasing their mobility and subsequent diffusion through the sediments (Huerta-Diaz and Morse, 1992). The higher Cd/Al and Cd/Ti ratios in the phosphate nodules support other indications of more pronounced conditions of anoxia during phosphogenesis.

- **Stable Carbon and Sulfur Isotopes**

– ***Carbon isotopes in carbonate-fluorapatite:*** Negative $\delta^{13}C$ values are found in the CO_3 of the carbonate-fluorapatite (CFA) of the phosphate nodules (Unit BH1), ranging from -1.23 to -0.86 ‰ (VPDB) (Al-Bassam, 2018, Table 8). These values are compatible with $\delta^{13}C$ values found in carbonate-fluorapatites deposited in the anoxic Cretaceous marine upwelling systems (Kolodny and Kaplan 1970; Al-Bassam, 1980; McArthur *et al*., 1980; Shemesh *et al*., 1988; Stolper and Eiler, 2016). They are lower than the $\delta^{13}C$ values reported by El-Shazly *et al*. (2011) in calcites of Cenomanian and Turonian age in the BCB and lower than the global mid-Cretaceous values for carbonates (Veizer and Hoefs, 1976). The negative carbon isotope values indicate significant enrichment of the light isotope of carbon (^{12}C) in the structural CO_3^{2-} of the CFA in the phosphate nodules relative to carbonates of comparable age. Using the estimates of Veizer and Hoefs (1976) for carbonates deposited in normal marine conditions, the δ13C for the C/T marine carbonates deposited around (93 – 94 Myr) should be +2.2‰ (VPDB). This value is higher than the $\delta^{13}C$ reported for the CO_3 in the studied CFA by about 3‰ to 4‰ (VPDB). The enrichment in the light isotope of carbon indicates organic source, which can be supplied by the bacterial disintegration of organic matter in the pore water environment, below sediment-water interface (e.g., Arning *et al*., 2009; Hiatt *et al*., 2015). In the studied case, such model suggests reducing conditions of phosphogenesis, similar to those found in marine upwelling systems (e.g., Kolodny and Kaplan 1970; McArthur *et al*., 1980; Stolper and Eiler, 2016).

– ***Sulfur isotopes in pyrite:*** The sulfur isotope analysis of a pyritized bivalve shell, collected from Unit P3 of the Pecínov Member, provides further evidence of anoxia with a low $\delta^{34}S$ value of -25‰ (CDT). Similarly, low $\delta^{34}S$ values in pyrite are recorded elsewhere in the OAE 2 black shales (Hetzel *et al*., 2009). These values correspond to bacterial sulfate reduction and subsequent pyrite formation (Arning *et al*., 2009) which attests to the anoxic conditions prevailed during the OAE 2 in the Pecínov section.

Table 8: Carbon and sulfur stable isotope composition

Material and references	$\delta^{13}C$ (‰ VPDB)	$\delta^{34}S$ (‰ CDT)
Apatite in Unit BH1 (Al-Bassam, 2018)	-1.23 to -0.86	
Calcite in Cenomanian rudist shells (El-Shazly *et al.*, 2011)	-0.54 to +4.3	
Calcite in Turonian rudist shells (El-Shazly *et al.*, 2011)	+3.13	
Pyrite in Unit P3 (Al-Bassam *et al*., 2019)		- 25

- **Microbial Signature**

Phosphatized fossil biomorphs have been identified by detailed SEM examination and EDX microanalysis in the phosphate nodules of Unit BH1 (Al-Bassam and Halodová, 2018). They are < 1 – 3 μm in size and form integral parts of the textural constituents of the phosphate nodules (Fig.6). They show biological filaments, rods, cellular strings of microbial forms and colonial associations and found in cavities as intrinsic parts of the rock constituents. They were identified as chemotrophic sulfur-reducing fossil bacteria by Al-Bassam and Halodová (2018), similar to modern and ancient analogues (e.g. Hiatt *et al*., 2015). The type and habitat of these fossil bacteria in the phosphate nodules indicate anoxic conditions during phosphogenesis (Arning, *et al*., 2009 and references therein).

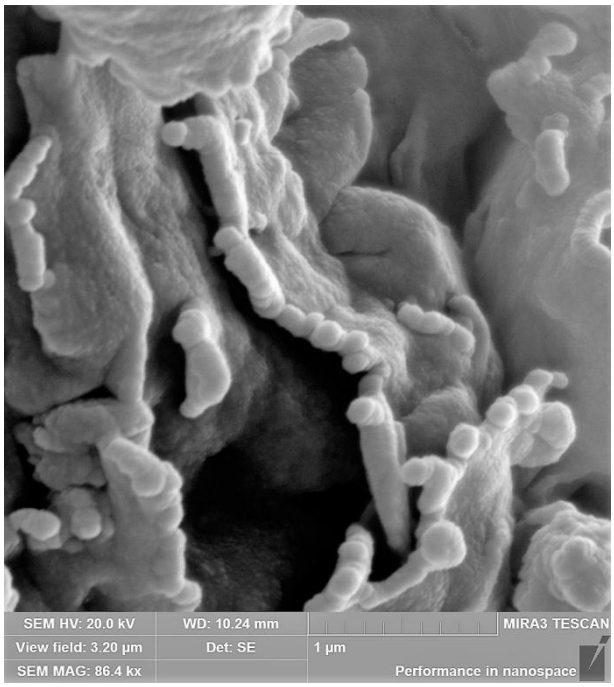

Fig.6: Cellular strings of fossil sulfur-reducing bacteria in phosphate nodules (see Al-Bassam and Halodová, 2018 for details)

- **Geochemical compatibility with the $\delta^{13}C_{org}$ profile**

The results of $\delta^{13}C$ obtained in this study are compared to the $\delta^{13}C$ values analysed in organic matter and reported in Uličný *et al.* (1997) and Košťák *et al*. (2018) for the Pecínov OAE 2 section (Fig.2). The $\delta^{13}C_{org}$ profile is not uniform in the Pecínov section and shows minimum value of (-27‰) and a maximum value of (-21.5‰) (Fig.2). Sharp major $\delta^{13}C_{org}$ excursion (~ +4‰) is found at the base of Unit P3 and was stratigraphically compared to peak

"b" of the OAE 2 (Košťák *et al*., 2018). Lower magnitude and broader $\delta^{13}C_{org}$ positive humps were detected in units P3 and P4 ranging (-24 – -23 ‰).

At the base of Unit P3, sample 23A coincides with the highest $\delta^{13}C_{org}$ value of (~ -21.5‰) (Fig.2) which represent the lower part of peak "b" of the OAE 2 in this section (Košťák *et al*., 2018). This sample shows the highest values of Ce-anomaly, Ce/La, Ni/Al, Ni/Ti, Co/Al and Co/Ti ratios relative to other Cenomanian and Turonian mudstone samples (Tables 1 – 3). It also shows the highest TOC content (0.89 wt.%), apatite content (22.5 modal %), Ce, La, Nd, Ni and Co concentrations coupled with the lowest S_{tot}, Zn and Cd concentrations. Nickel, Co and REE indices are the most expressive indicators of anoxia in this case. On the other hand, other redox sensitive trace elements and their Al- and Ti-normalized ratios are present in near average values. The overlying sample (24A) coincides with the upper part of the $\delta^{13}C$ peak "b" (Fig.2). It represents an Al- and Ti-rich claystone bed (Al = 13.85 wt.% and Ti = 0.58 wt.%) with high contents of smectite and kaolinite and low content of TOC (0.56 wt.%). It shows the lowest values of Al- and Ti-normalized redox sensitive TE's, Fe indices and REE indices. The depleted Mn/Al ratio and elevated Cu/Al and Cu/Ti ratios are the only indicators of anoxia in this sample, whereas Fe_{tot}/Al, Co/Al, Ni/Al, Cd/Al, Cd/Ti; Ce/La ratios and Ce-anomaly show the lowest values among the mudstone samples. The relative depletion of TE's in this sample may be linked with the low TOC content, whereas the lower values of most Al- and Ti-normalized redox indices can be attributed to the high Al and Ti concentrations.

Sample 7A is located at the upper part of Unit P3 and coincides with relatively elevated $\delta^{13}C_{org}$ values of (~ 23.5‰) (Fig.2). This sample shows depleted concentrations of REE, elevated concentration of Fe, Mn and Cu, and elevated values of Fe_{tot}/Al, Fe^{2+}/Fe_{tot}, Mn/Al, Cu/Al, Mn/Ti and Cd/Ti ratios relative to other samples of Unit P3. Despite the relatively higher values of Mn concentration and Mn/Al and Mn/Ti ratios in this sample, these indices are still much lower than those in average shale (Tables 1, 4). Significant Mn mobilization under suboxic conditions is supported by the higher values of other redox indices, such as $Fe^{2+/}Fe/_{tot}$, Fe_{tot}/Al, Cu/Al and Cd/Ti, which are compatible with the $\delta^{13}C_{org}$ profile. Within Unit P4, the $\delta^{13}C_{org}$ profile shows elevated broad hump of about (-23.5 ‰) which coincides with samples 8A, 9A and 10A of this study (Fig.2). These samples show variable values of redox indices; the suboxic characters are mainly demonstrated in sample 9A, where relatively higher values of Ce-anomaly, Ce/La, Ni/Al, Zn/Al and Cd/Al ratios are found in association with higher Fe^{2+} concentration (Table 1). Higher concentrations of Ni, Zn, Cd, La and Ce, and Zn/Al and Zn/Ti ratios are found in sample 10A, whereas higher concentration of TOC, S_{tot}, and Fe_{tot}/Al ratios are found in sample 8A. Among these indices, $Fe^{2+}/Fe_{tot,}$ Zn/Al and Zn/Ti are the most compatible with the $\delta^{13}C_{org}$ profile.

The upper and most pronounced $\delta^{13}C$ excursion, globally identified in organic matter, bulk rock and carbonates, as peak "c" (Jarvis *et al*., 2006), is missing in the $\delta^{13}C_{org}$ profile of the Pecínov section due to erosion caused by an extreme shallowing event at the C/T boundary (Košťák *et al*., 2018, Fig.2). Most of the phosphate nodules hosted now in Unit BH1 were reworked from older (latest Cenomanian) horizon(s), matured during this shallowing event and mechanically emplaced in the overlying early Lower Turonian unit BH1 (Laurin, 1996; Uličný *et al*., 1997; Al-Bassam and Magna, 2018 and Al-Bassam *et al*., 2019). Bleaching of the outer surface of these nodules, borings penetrating some of them and the sharp contact with the mudstone host (Fig.4) indicate reworking. The heterogenic character of Unit BH1 is supported by geochemical criteria, shown in the wider range of TE's concentrations and geochemical indices found in the mudstones of this unit compared to those

in units P3 and P4. Most probably the phosphate nodules were originally developed within that missing part of the sequence holding the characters of the peak "c" $\delta^{13}C$ excursion at the C/T boundary. Consequently, they should have preserved the original signature of this anomalous anoxic event. This is indicated by the highest REE indices of anoxia found in the phosphate nodules and the highest redox-sensitive TE's normalized to Al and Ti among all samples. It is also supported by the negative $\delta^{13}C$ values of the CO_3 in the apatite structure and by the sulfur-reducing type of bacteria, dominating the fossil microbial community in these phosphate nodules.

CONCLUSIONS

- The positive Ce-anomaly values and the > 2 Ce/La ratios in all mudstone samples of units P3, P4 and BH1confirm the generally suboxic–anoxic conditions prevailed during most of the OAE 2 time span in the Pecínov section. Nickel, Co and REE indices are the most expressive inorganic geochemical indicators of anoxia in the case studied. This is complemented by the low Mn concentration in the mudstones, the negative values of $\delta^{13}C$ of CFA and $\delta^{34}S$ of pyrite and by the dominant fossil sulfur-reducing type of bacteria in the phosphate nodules.
- Some redox-sensitive geochemical indicators in the Pecínov section show compatibility with the $\delta^{13}C_{org}$ profile in having anomalous values at the base of Unit P3 that may be related to peak "b" of the OAE 2 and anomalous indices of anoxia in the phosphate nodules which may be the signature of peak "c" of this anoxic event.
- The relatively low concentration of TOC and most of the redox sensitive and sulfide-residing TE's in the Pecínov section can be related to frequent shallowing and oxygenation episodes, indicated by multiple omission surfaces coupled with bioturbation structures. Shallowing events frequently interrupted the stagnant reducing bottom environment and decreased equilibrium mixing with open marine water, which resulted in the depletion of TOC and the subsequent mobilization of significant part of the TE's bound to organic material outside the sedimentary system.
- Truly anoxic conditions must have been short lived or less preserved events in the Pecínov section, where the variation in the redox-sensitive TE's along most of the studied OAE 2 sequence is often controlled by mineralogy. Mineral constrains have occasionally overprinted the original anoxic geochemical signature following the oxidation of TE-rich organic matter in frequent shallowing oxic events.
- There is no consistent geochemical facies characterizing the OAE 2 signature in the black shales of the European and the Atlantic Ocean sections reported in this study. The inconsistency is shown in the highly variable TOC content and wide range values of redox indices derived from redox-sensitive elements.

ACKNOWLEGMENTS

This work is part of the internal research project no. 321620 sponsored by the Czech Geological Survey (CGS), Prague. Field sampling at the Pecínov quarry was carried out with the help and guidance of Dr. Stanislav Čech, senior stratigrapher at CGS.

REFERENCES

Adams, D.D., Hurtgen, M.T. and Sageman, B.B., 2010. Volcanic triggering of a biogeochemical cascade during Oceanic Anoxic Event 2. Nature Geosciences, Vol.3, p. 201 – 204.

Al-Bassam, K.S., 1980. Carbon and oxygen isotope composition of some marine sedimentary apatites from Iraq. Economic Geology, Vol.75, p. 1231 – 1233.

Al-Bassam, K.S., 2018. Stable carbon and oxygen isotopes of some carbonate-fluorapatites from Cenomanian and Turonian sequences, Bohemian Cretaceous Basin, Czech Republic. Iraqi Geological Journal, Vol.51, No.1, p. 1 – 16.

Al-Bassam, K.S. and Halodová, P., 2018. Fossil bacteria in Cenomanian – Turonian phosphate components, Bohemian Cretaceous Basin, Czech Republic. Annales Societatis Geologorum Poloniae. Vol.88, No.33, p. 257 – 272

Al-Bassam, K.S. and Magna, T., 2018. Distribution and significance of rare earth elements in Cenomanian–Turonian phosphate components and mudstones from the Bohemian Cretaceous Basin, Czech Republic. Bulletin of Geosciences, Vol.93, No.3, p. 347 – 368

Al-Bassam, K.S. Magna, T., Vodrážka, R. and Čech, S., 2019. Mineralogy and geochemistry of marine glauconitic siliciclasts and phosphates in selected Cenomanian – Turonian units, Bohemian Cretaceous Basin, Czech Republic: Implications for provenance and depositional environment. Geochemistry, Vol.79, p. 347 – 368.

Al-Dulaimy, A.S. and Awadh, S.M., 2007. Geochemical and Paleontological study of Gulneri Formation (Upper Cretaceous), NE Iraq. Journal of the University of Anbar for Pure Science., Vol.1, No.3, p. 64 – 74 (in Arabic).

Algeo, T.J., and Maynard, J.B., 2004. Trace-element behavior and redox facies in core shales of Upper Pennsylvanian Kansas-type cyclothems. Chemical Geology, Vol.206, No. 3 – 4, p. 289 – 318.

Algeo, T.J., Lyons, T.W., Blakey, R.C., and Over, D.J., 2007. Hydrographic conditions of the Devono–Carboniferous North American Seaway inferred from sedimentary Mo–TOC relationships. *Palaeogeography, Palaeoclimatology, Palaeoecology*, Vol.256, No. 3 – 4, p. 204 – 230.

Al-Sheikhly, S.S., Tamar-Agha, M.Y. and Mahdi, M.M., 2015. The facies analysis of the Cenomanian – Turonian succession of Surdash – Shaqlawa area, NE Iraq. Iraqi Jour. Sci., Vol.56, No.1C, p. 767 – 773.

Altschuler, Z.S. 1980. The geochemistry of trace elements in marine phosphorites. Society for Sedimentary Geology (SEPM) Special Publications, Vol.29, p. 19 – 30.

Arning, E.T., Birgel, D, Brunner, B. and Peckmann, J. 2009. Bacterial formation of phosphatic laminites off Peru. Geobiology, Vol.7, No.3, p. 295 – 307.

Arthur, M.A., Dean, W.E. and Schlanger, S.O., 1985. Variations in the global carbon cycle during the Cretaceous related to climate, volcanism and changes in atmospheric CO2. In: Sundquist, E.T., Broecker, W.S. (Eds.). The carbon cycle and atmospheric CO2: Natural variations archean to present. AGU Geophysical Monograph, Vol.32, p. 504 – 529.

Arthur, M.A., Schlanger, S.O. and Jenkyns, H.C., 1987. The Cenomanian – Turonian oceanic anoxic event. II. Palaeoceanographic controls on organic-matter production and preservation. In: Brooks, J., Fleet, A.J. (Eds.), Marine Petroleum Source Rocks. Geological Society Special Publication, Vol.26, p. 401 – 420.

Arthur, M.A., Dean, W.E. and Pratt, L.M., 1988. Geochemical and climatic effects of increased marine organic carbon burial at the Cenomanian/ Turonian boundary. Nature, Vol.335, No.6192, p. 714 – 717.

Ackerman, L., Magna, T., Rapprich, V., Upadhyay, D., Krátký, O., Čejková, B., Erban, V., Kochergina, Yu.V. and Hrstka, T., 2017. Contrasting petrogenesis of spatialy related carbonatites from Samalpatti and Sevattur, Tamil Nadu, India. Lithos Vol. 284 – 285, p. 257 – 275.

Böning, P., Brumsack, H.-J., Böttcher, M.E., Schnetger, B., Kriete, C., Kallmeyer, J. and Borchers, S.L., 2004. Geochemistry of Peruvian near-surface sediments. Geochimica et Cosmochimica Acta, Vol.68, No.21, p. 4429 – 4451.

Brumsack, H.-J., 1989. Geochemistry of recent TOC-rich sediments from the Gulf of California and the Black Sea. Geologische Rundschau, Vol.78, No.3, p. 851 – 882.

Brumsack, H.-J., 2006. The trace metal content of recent organic carbon-rich sediments: implications for Cretaceous black shale formation. Palaeogeography, Palaeoceanography, Palaeoecology, Vol.232, No. 2 –4, p. 344 – 361.

Calvert, S.E., Pedersen, T.F., 1993. Geochemistry of Recent oxic and anoxic marine sediments: implications for the geological record. Marine Geology, Vol.113, p. 67 – 88.

Čech, S., Klein, V., Kříž, J. and Valečka, J., 1980. Revision of the Upper Cretaceous stratigraphy of the Bohemian Cretaceous Basin. Věstnik Ústředniho Ústavu Geologického, Vol.55, No.5, p. 277 – 296.

Čech, S., Hradecká, L., Svobodová, M. and Švábenická, L., 2005. Cenomanian and Cenomanian – Turonian boundary in the southern part of the Bohemian Cretaceous Basin, Czech Republic. Bulletin of Geosciences, Vol.80, No.4, p. 321 – 354.

Cruse, A.M., and Lyons, T.W., 2004. Trace metal records of regional paleoenvironmental variability in Pennsylvanian (Upper Carboniferous) black shales. Chemical Geology, Vol.206, No. 3 – 4, p. 319 – 345.

Curiale, J.A. 1993. Geochemical anomalies at the Cenomanian – Turonian boundary, northwest New Mexico. Organic Geochemistry, Vol.22, No. 3 – 5, p. 487 – 500.

Dempírová, L., Šikl J., Kašičková, R., Zoulková, V. and Kříbek, B. 2010. The evaluation of precision and relative error of the main components of silicate analyses in Central Laboratory of the Czech Geological Survey. Geoscience Research Reports, Vol.43, p. 326 – 330.

Dobeš, P., Povondra, P. and Kühn, P., 1987. Mineralogie a geochemie fosforitů české křídové pánve (in Czech with English summary). Acta Universitatis Carolinae Geology, Vol.54, p. 145 – 170.

Du Vivier, A.D.C., Selby, D, Sageman, B.B., Jarvis, I. Grocke, D.R. and Voigt, S., 2014. Marine Os-187/Os-188 isotope stratigraphy reveals the interaction of volcanism and ocean circulation during Oceanic Anoxic Event 2. Earth and Planetary Science Letters, Vol.389, p. 23 – 33.

Elder, W.P. 1989. Molluscan extinction patterns across the Cenomanian – Turonian stage boundary in the Western Interior of the United States. Paleobiology, Vol.15, p. 299 – 320.

El-Shazly, S., Košťák, M., Abdel-Gawad, G., Kloukčová, B., Saber, S.G., Salama, Y.F., Mazuch, M. and Žák, K. 2011. Carbon and oxygen stable isotopes of selected Cenomanian and Turonian rudists from Egypt and Czech Republic, and a note on changes in rudist diversity. Bulletin of Geosciences, Vol.86, No.2, p. 209 – 226.

Erbacher, J., Thurow, J. and Littke, R., 1996. Evolution patterns of radiolaria and organic matter variations: a new approach to identify sea-level changes in Mid-Cretaceous pelagic environments. Geology, Vol.214, p. 499 – 502.

Forster, A., Schouten, S., Moriya, K., Wilson, P. A., and Sinninghe Damst´e, J. S., 2007. Tropical warming and intermittent cooling during the Cenomanian/ Turonian oceanic anoxic event 2: Sea surface temperature records from the equatorial Atlantic, Paleoceanography, 22, PA1219, doi:10.1029/2006pa001349.

Gangl, S.K., Moy C.M., Stirling, C.H., Jenkyns, H.C., Crampton, J.S., Clarkson, M.O.., Ohneiser, C. and Porcelli, D., 2019. High-resolution record s of Oceanic Anoxic Event 2: Insights into the timing, duration and extent of environmental perturbations from the palaeo-South Pacific Ocean. Earth and Planetary Science Letters, Vol.518, p. 172 – 182

German, C.R. Holliday, B.P. and Elderfield, H. 1991. Redox cycling of rare earth elements in the suboxic zone of the Black Sea. Geochimica et Cosmochimica Acta, Vol.55, p. 3553 – 3558.

Haskin, M.A. and Haskin, L.A., 1966. Rare earths in Europian shales: a redetermination. Science, Vol.154, p. 507 – 509.

Hetzel, A., 2009. Geochemical signatures of black shales deposited during Oceanic Anoxic Event 2 (Cenomanian/Turonian) in the tropical Atlantic (Demerara Rise, ODP Leg 207) and in northern Germany (Wunstorf). Ph.D Thesis, Universität Oldenburg zur Erlangung des Grades und Titels einer, Germany. 228pp.

Hetzel, A., Brumsack, H-J., Böttcher, M.E. and Schnetger, B., 2006. Inorganic geochemical characteriziation of lithologic units recovered during ODP Leg 207 (Demerara Rise). In: Mosher, D.C., Erbacher, J., Malone, M.J. (Eds.), Proceedings of the Ocean Drilling Program, Scientific Results, College Station, TX (Ocean Drilling Program), Vol.207, p. 1 – 37.

Hetzel, A., Böttcher, M.E., Wortmann, U.G. and Brumsack, H.-J., 2009. Paleo-redox conditions during OAE 2 reflected in Demerara Rise sediment geochemistry (ODP Leg 207). Palaeogeography, Palaeoceanography, Palaeoecology, Vol. 273, No. 3 – 4, p. 302 – 328.

Hetzel, A., M¨arz, C., Vogt, C., and Brumsack, H-J. 2011. Geochemical environment of Cenomanian – Turonian black shale deposition at Wunstorf (northern Germany), Cretaceous Res., Vol.32, p. 480 – 494.

Hiatt, E.E., Pufahl, P.K. and Edwards, C.T., 2015. Sedimentary phosphate and associated fossil bacteria in a Paleoproterozoic tidal flat in the 1.85Ga Michigamme Formation, Michigan, USA. Sedimentary Geology, Vol.319, p. 24 – 39.

Høgdahl, O.T., Melsom, S. and Bowen, V.T. 1968. Neutron activation analysis of lanthanide elements in sea water. American Chemical Society, Vol.73, p. 308 – 325.

Huerta-Diaz, M.A. and Morse, J.W., 1992. Pyritization of trace metals in anoxic marine sediments. Geochim. Cosmochim. Acta, Vol.56, p. 2681 – 2702.

Jarvis, I., Gale, A.S., Jenkyns, H.C. and Pearce, M.A. 2006. Secular variation in Late Cretaceous carbon isotopes: a new δ13C carbonate reference curve for the Cenomanian – Campanian (99.6-70.6Ma). Geological Magazine, Vol.143, p. 561 – 60

Jarvis, I., Lignum, J.S., Gr¨ocke, D.R., Jenkyns, H.C., and Pearce, M.A., 2011. Black shale deposition, atmospheric CO2 drawdown, and cooling during the Cenomanian – Turonian Oceanic Anoxic Event, Paleoceanography, Vol.26, PA3201, doi: 10.1029/2010pa002081

Kauffman, E.G., 1984. The fabric of Cretaceous marine extinctions. In: W. Berggren and J. Van Couvering (Eds.), Catastrophes in Earth History. The uniformitarianism. Princeton University Press, Princeton, USA, p. 151 – 246.

Kear, B.P., Ekrt, B., Prokop, J. and Georgalis, G., 2013. Turonian marine amniotes from the Bohemian Cretaceous Basin, Czech Republic. Geological Magazine, Cambridge University Press/ online: doi: 10.1017/S0016756813000502

Kerr, A.C., 1998. Oceanic plateau formation: a cause of mass extinction and black shale deposition around the Cenomanian – Turonian boundary? Jour. Geol. Soc. London, Vol.155, p. 619 – 626.

Kolodny, Y. and Kaplan, I.R., 1970. Carbon and oxygen isotopes in apatite-CO2 and co-existing calcite from sedimentary phosphorite. Jaournal of Sedimentary Petrology, Vol.40, p. 954 – 959.

Košťák, M., Čech, S., Uličný, D., Sklenář, J., Ekrt, B., Mazuch, M., 2018. Ammonites, inoceramids, and stable carbon isotopes of the Cenomanian – Turonian OAE2 interval in Central Europe: Pecínov quarry, Bohemian Cretaceous Basin (Czech Republic). Cretaceous Research. Vol.87, p. 150 – 173.

Kuhnt, W., Luderer, F., Nederbragt, S., Thurow, J. and Wagner, T., 2005. Orbital-scale record of the late Cenomanian–Turonian oceanic anoxic event (OAE-2) in the Tarfaya Basin (Morocco). Int. J. Earth Sci., Vol.94, p. 147 – 159.

Kuroda, J. Ogawa, N., Tanimizu, M., Coffin, M.F., Tokuyama, H., Kitazato, H. and Ohkouchi, N., 2007. Contemporaneous massive subaerial volcanism and late Cretaceous Oceanic Anoxic Event 2. Earth Planet Sci. Lett., Vol.256, p. 211 – 223.

Kuypers, M.M., Pancost, R.D., Nijenhuis, I.A. and Sinninghe Damsté, J.S., 2002. Enhanced productivity led to increased organic carbon burial in the euxinic North Atlantic basin during the late Cenomanian oceanic anoxic event. Paleoceanography, Vol.17, 1051. https://doi .org /10 .1029 /2000PA000569

Laurin, J., 1996. Sedimentary discontinuities with evidences of phosphatic mineralization as a record of the changes of sea level; Bohemian Cretaceous Basin. Diploma thesis (in Czech), Charles University. Prague, 122pp.

Marlof, N.J., 2014. Redox-Sensitive Trace Elements Document Chemical Depositional Environment and Post-Depositional Oxidation of the Ediacaran Biri Formation, Southern Norway MSc. Thesis, Department of Geosciences, Colorado State University, Fort Collins, Colorado, USA, 102pp.

McArthur, J.M., Coleman, M.L. and Bremner, J.M., 1980. Carbon and oxygen isotopic composition of structural carbonate in sedimentary francolite. Journal of the Geological Society of London, Vol.137, p. 669 – 673.

McCrea, J.M., 1950. On the isotopic Chemistry of carbonates and paleotemperatur scale. Journal of Chemical Physics, Vol.18, p. 849 – 857.

Mitchell, R. N., Bice, D. M., Montanari, A., Cleaveland, L. C., Christianson, K. T., Coccioni, R., and Hinnov, L. A., 2008. Oceanic anoxic cycles? Orbital prelude to the Bonarelli Level (OAE 2), Earth Planet. Sci. Lett., Vol.267, p. 1 – 16.

Monteiro, F., Pancost, R., Ridgwell, A. and Donnadieu, Y., 2012. Nutrients as the dominant control on the spread of anoxia and euxinia across the Cenomanian – Turonian oceanic anoxic event (OAE2): model-data comparison. Paleoceanography, Vol.27, PA4209. https://doi .org /10 .1029 /2012PA002351.

Orth, C.J., Attrep, M. Jr., Mao, X.Y., Kauffman, E.G., Diner, R. and Elder, W.P., 1988. Iridium abundance maxima in the Upper Cenomanian extinction interval. Geophysical Research Letters, Vol.15, p. 346 – 349.

Orth, C.J., Attrep, M. Jr., Quintane, L.R., Elder, W.P., Kauffman, E.G., Diner, R. and Villamil, T., 1993. Elemental abundance anomalies in the Late Cenomanian extinction interval: a search for the source(s). Earth and Planetary Science Letters, Vol.117, p. 189 – 204.

Piper, D.Z. 1974. Rare earth elements in the sedimentary cycle: A summary. Chemical Geology, Vol.14, p. 285 – 304.

Piper, D.Z. and Bau, M. 2013. Normalized rare earth elements in water, sediments and wine: identifying sources and environmental redox conditions. American Journal of Analytical Chemistry, Vol.4, p. 69 – 83.

Pogge von Strandmann, P.A.E., Jenkyns, H.C. and Woodfine, R.G., 2013. Lithium isotope evidence for enhanced weathering during Oceanic Anoxic Event 2. Nature Geosciences, Vol.6, p. 668 – 672.

Pratt, L.M., Force, E.R. and Pomerol, B., 1991. Coupled manganese and carbon-isotope events in marine carbonates at the Cenomanian – Turonian boundary. Journal of Sedimentary Petrology, Vol.61, p. 370 – 383.

Schieber, J., 1994. Evidence for high-energy events and shallow-water deposition in the Chattanooga Shale, Devonian, central Tennessee, USA. Sedimentary Geology, Vol.93, No. 3 – 4, p. 193 – 208.

Schlanger, S. and Jenkyns, H., 1976. Cretaceous oceanic anoxic events: causes and con-sequences. Geologie en Mijnbouw, Vol.55, p. 179 – 194.

Scholle, P.A. and Arthur, M.A., 1980. Carbon isotope fluctuations in Cretaceous pelagic limestones: Potential stratigraphic and petroleum exploration tool. Bull. Amer. Assoc. Petroleum Geol., Vol.64, p. 67 – 87.

Shemesh, A., Kolodny, Y. and Luz, B. 1988. Isotope geochemistry of oxygen and carbon in phosphate and carbonate of phosphorite francolite. Geochimica et Cosmochimica Acta, Vol.52, p. 2565 – 2572.

Shields, G.A. and Stille, P. 1998. Stratigraphic trends in cerium anomaly in authigenic marine carbonates and phosphates: diagenetic alteration or sedimentary signals? Goldschmidt Conference, Toulouse, 1998, p. 1387 – 1388, ULP-EOST-CNRS, Centre de Geochimie de la Surface, UMR 7517, Strasbourg, France.

Stolper, D.A. and Eiler, J.M., 2016. Constraints on the formation phosphorites using carbonate clumped isotopes. Geochimica et Cosmochimica Acta. http://dx.doi.org/10.1016/j.gca.2016.02.030

Thurow, J., Brumsack, H.-J., Rullkötter, J., Littke, R. and Meyers, P., 1992. The Cenomanian/ Turonian boundary event in the Indian Ocean - a key to understand the global picture. In: R.A. Duncan, D.K. Rea, R.B. Kidd, U. von Rad and J.K. Weissel (Eds.), The Indian Ocean: A Synthesis of Results from the Ocean Drilling Program. American Geophysical Union, Geophysical Monograph, Vol.70, p. 253 – 273.

Tourtelot, H., 1979. Black shale – its deposition and diagenesis. Clays and Clay Minerals, Vol.27, No.5, p. 313 – 321

Tribovillard, N., Algeo, T.J., Lyons, T. and Riboulleau, A., 2006. Trace metals as paleoredox and paleoproductivity proxies: An update. Chemical Geology, Vol. 232, No. 1– 2, p. 12 – 32.

Turekian, K. K. and Wedepohl, K. H., 1961. Distribution of the elements in some major units of the Earth's crust. Geol. Soc. Amer. Bull., Vol.72, p. 175 – 192.

Turgeon, S. and Brumsack, H.-J., 2006. Anoxic vs dysoxic events reflected in sediment geochemistry during the Cenomanian-Turonian Boundary Event (Cretaceous) in the Umbria-Marche Basin of central Italy. Chemical Geology, Vol.23, No. 3 – 4, p. 321 – 339.

Ugata, D.B.P., 2007. Glauconite as an indicator of sequence stratigraphic packages in a Lower Paleocene passive-margin shelf succession, central Alabama. M.Sc. Thesis, Auburn University, Alabama, USA, 109pp.

Uličný, D., 1997. Sedimentation in a reactivated intra-continental strike-slip fault zone: The Bohemian Cretaceous Basin, Central Europe. Gaea heidelbergensis, 3, Abstracts, 18th IAS Regional Europian Meeting, Heidelberg, 347pp.

Uličný, D., 2001. Depositional systems and sequence stratigraphy of coarse-grained deltas in a shallow-marine, strike-slip setting: the Bohemian Basin, Czech Republic. Sedimentology, Vol.48, p. 599 – 628.

Uličný, D., Hladíková, J., Attrep Jr., M.J., Čech, S., Hradecká, L. and Svobodová, M. 1997. Sea-level changes and geochemical anomalies across the Cenomanian-Turonian boundary: Pecínov quarry, Bohemia. Palaeogeography, Palaeoclimatology, Palaeoecology, Vol.132, p. 265 – 285.

Uličný, D., Špičáková, L., Grygar, R., Svobodová, M., Čech, S. and Laurin, J., 2009. Palaeodrainage systems at the basal unconformity of the Bohemian Cretaceous Basin: roles of inherited fault systems and basement lithology during the onset of basin filling. Bulletin of Geosciences, Vol.84, No.4, p. 577 – 610.

Valečka, J. and Skoček, V., 1991. Late Cretaceous lithoevents in the Bohemian Cretaceous Basin, Czechoslovakia. Cretaceous Research, Vol.12, p. 561 – 57.

Veiser, J. and Hoefs, J., 1976. The nature of O^{18}/O^{16} and C^{13}/C^{12} secular trends in sedimentary carbonate rocks. Geochimica et Cosmochimica Acta, Vol.40, p. 1387 – 1395.

Vogt, S., Erbacher, J., Mutterlose, J. Weisds, W., Westerhold, T., Weiss, F., Wilmsen, M. and Wonik, T., 2008. The Cenomanian – Turonian of the Wunstorf section (North Germany): global stratigraphic reference section and new orbital time scale for Oceanic Anoxic Event 2. Newsletters 1139 on Stratigraphy, Vol.43, No.1, p. 65 – 89.

Wright, J. Schrader, H. and Holser, W.T., 1987. Paleoredox variations in ancient oceans recorded by rare earth elements in fossil apatite. Geochimica et Cosmochimica Acta, Vol.51, p. 631 – 644.